Open Access

Catalysis Research

LIDSEN Publishing Inc.

Research Article

Co^{2+} Doping and Molecular Adsorption Behavior of Anatase TiO_2 (001) Crystal Plane

Jiarui Fang †, Ziheng Li †, *, Xiruo Bai †, Yichu Zhang †, Jiahui Liu †, Dan Wang †, Ye Yao †

Key Laboratory of Physics and Technology for Advanced Batteries, College of Physics, Jilin University, Changchun 130012, P. R. China; E-Mails: 977409249@qq.com; liziheng@jlu.edu.cn; 2876942723@qq.com; 981787105@qq.com; 799086706@qq.com; wdan0223@163.com; yeyao@jlu.edu.cn

† These authors contributed equally to this work.

* **Correspondence:** Ziheng Li; E-Mail: liziheng@jlu.edu.cn

Academic Editor: Ermelinda Falletta

Special Issue: Recent Advances in TiO2 Photocatalysis and Applications

Catalysis Research
2022, volume 2, issue 3
doi:10.21926/cr.2203018

Received: May 10, 2022
Accepted: June 26, 2022
Published: July 05, 2022

Abstract

TiO_2 (001) crystal plane exhibits molecular adsorption and photocatalytic activity. The loading capacity of reactive oxygen species present on crystal planes helps in the significant improvement of catalytic activity. The methods of synthesis and conditions of existence significantly affect the molecular adsorption properties of crystal planes, which in turn affects the ability of the system to load reactive oxygen species. Herein, we report the simulation of the molecular adsorption behavior on the TiO_2 (001) using the density functional theory technique. The results show that the crystal plane doped with Co^{2+} produces an oxygen defect and chemisorbs O_2 molecules present in the vicinity. Under conditions of adequate O_2 concentration, the second O_2 molecule is chemisorbed. This significantly improves the ability of the crystal plane to store oxygen. However, the undoped planes adsorb H_2O molecules and undergo hydroxylation under the synthesis and processing conditions. The ability to adsorb O_2 molecules is poor. The doping of Co^{2+} increases the electrical conductivity of the crystal

plane and the electrical sensitivity of adsorbed O_2 molecules, which is beneficial to the further improvement of the catalytic activity of the system. Fourier transform infrared spectroscopy (FTIR), and electrochemical impedance spectroscopy (EIS) techniques were used to confirm these results. The results indicate that the adsorption capacity of O_2 present on the TiO_2 (001) crystal plane can be changed by Co^{2+} doping to improve the catalytic activity of the crystal plane.

Keywords
TiO_2-Co; doping; adsorption; characteristic adsorption species; density functional theory

1. Introduction

In recent years, gas sensors have attracted immense attention as they are safe and can be used to address several environmental issues [1, 2]. The adsorption properties of gas molecules present on crystal planes are being increasingly studied in recent times [3-5]. Many metal-based semiconductor oxides have been used to research gas-sensitive materials, such as SnO_2, ZnO, and TiO_2. TiO_2 has become a hot spot in the research of gas sensor materials in recent years as it is non-toxic and is characterized by high activity and good chemical stability [6-15]. TiO_2 presents three structures: anatase, rutile, and brookite. Anatase TiO_2 exhibits good catalytic activity, and hence studies on anatase TiO_2 are being widely conducted.

The surface structure of nano TiO_2 has been reported. Theoretical and experimental studies revealed that the (001) crystal plane of the anatase TiO_2 unit is characterized by high plane energy [16, 17]. According to the first principle, the plane (001) contains a strong, active oxygen adsorption site, which plays a great role in improving the adsorption performance of TiO_2 [18]. Wanbayor et al. used the density functional theory (DFT) technique to study the adsorption strength of CO, H_2, N_2, NH_3, and CH_4 on TiO_2 (001) and (101) planes [19]. It has been reported that the doping of metal elements in TiO_2 as additives can help improve the gas adsorption performance of the systems. Through first-principles calculation, Lin et al. doped precious metal on the plane of the TiO_2 crystal to form oxygen vacancies, resulting in stable CH_4 adsorption [20]. Abbasi et al. studied the interaction between Au-supported TiO_2 nanoparticles and NO_2 using the DFT technique. The results provide a platform for studying the gas sensing properties of TiO_2 nanomaterials [21].

The mechanism associated with the adsorption of TiO_2 clusters on planes has been previously studied. F. Aguilera-Granja et al. studied the process of adsorption of stable TiO_2 clusters on graphene, silver, and gold using the DFT technique [22]. D.V. Potapenko et al. reported the atomic resolution of TiO_2 nanocrystals adsorbed under conditions of photoreaction [23]. It has also been reported that the presence of metal clusters can improve the adsorption capacity of TiO_2 [24-26]. We studied the effect of metal ion doping on the electrical properties of TiO_2 (001) crystal planes by comparing the adsorption behavior of gas molecules on undoped TiO_2 and Co^{2+} ion-doped TiO_2 (001) crystal planes.

Herein, the molecular adsorption behaviors of TiO_2 (001) and TiO_2-Co (001) crystal planes are reported. The characteristic adsorption species of the TiO_2 (001) crystal plane and TiO_2-Co (001) crystal plane are determined using the DFT technique, and the molecular adsorption behavior of

the crystal plane is investigated under different environments using the electrochemical impedance spectroscopy technique. The results reveal that the process of Co^{2+} ion doping changes the electrical properties of the TiO_2 (001) crystal plane and improves the ability of the crystal plane to adsorb O_2. This provides a theoretical basis for the study of TiO_2 in the field of catalysis. The results can potentially help in the development of gas-sensitive materials.

2. Experimental

2.1 Preparation of the (001) Plane Exposed TiO_2 Sample

The anatase TiO_2 (001) plane is prepared following the hydrothermal synthesis method [27]. Tetrabutyl titanate (25 mL) is placed in a Teflon-lined autoclave with a capacity of 100 mL. Following this, 3 mL of hydrofluoric acid is dripped into the system under conditions of magnetic agitation. The mixture is stirred for half an hour, sealed in the autoclave, and heated in a drying oven at 180 °C for 24 h. following the completion of the hydrothermal reaction, the sample is removed from the autoclave and cooled down to room temperature(25°C). The precipitates are washed with anhydrous ethanol, NaOH solution (0.1 M), and deionized water several times and collected following the process of centrifugation. The product is dried in a drying oven at 60 °C over a period of >12 h. The product is ground and calcined in a muffle furnace at 500 °C for 2 h. Finally, white anatase TiO_2 (001) is obtained in the powdered form.

2.2 Co^{2+} Doping on the Surface of TiO_2

The methods of synthesis of Co^{2+}-doped TiO_2 and undoped TiO_2 are the same before the hydrothermal reaction. White TiO_2 (powder) is added to a solution of $Co(NO_3)_2{\cdot}6H_2O$ (10 mL, 10^{-6} mol/L), and the solution is centrifuged under conditions of vigorous stirring for 3 min. Following this, the product is washed and filtered with deionized water. The obtained samples are put into a drying oven at 60 °C for 6 h, and TiO_2 powder doped with Co^{2+} is obtained post grinding.

2.3 Measurements

An X-ray diffractometer (XRD; Japanese Rigaku Mini Flex 600) is used to characterize the crystal structure of the samples (Cu Kα, λ = 1.5418 Å). The scan range spanned the region from 20° to 80°, and the scanning speed was 20°/min. The surface structure of the sample is observed using a scanning electron microscope (SEM) [28]. Elemental distributions are observed using an energy-dispersive spectrometer (EDS, BRUKR QUANTAX 200). The molecular structure and chemical composition of the samples are analyzed using the Fourier transform infrared spectroscopy (FTIR) technique using potassium bromide as the substrate.

2.4 Electrochemical Impedance Spectroscopy (EIS)

An electrochemical workstation (CS2350) is used to perform AC impedance spectroscopy tests on samples under conditions of different atmospheres. The sample is evenly spread across the gap between the fingered electrodes, which are connected to the electrodes and placed in the test chamber. The single test time is 20 min, and the test range is 100 K to 0.1 Hz. The double electrode method is used to conduct the experiment. The working electrode and the counter electrode are

fixed at both ends of the fork finger electrode to form a loop. The equivalent circuits of undoped TiO_2 and TiO_2-Co samples are shown in Figure 1 (a) and Figure 1 (b), respectively. Rs, CPE, and Rp, are equivalent series resistance, double-layer resistance, and charge transfer resistance, respectively. C in Figure 1 (a) denotes capacitance. In Figure 1 (b), Ws is the Warburg impedance.

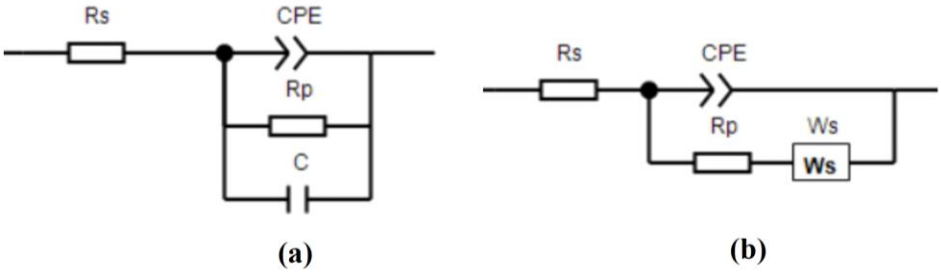

Figure 1 (a) Equivalent circuit diagram of undoped TiO_2; (b) Equivalent circuit diagram of TiO_2–Co.

2.5 Theoretical Simulation and Calculation Methods

Flake-like TiO_2 material is synthesized, and the structures are observed using the SEM technique. The micro and the bare crystals belong to the TiO_2 (001) crystal plane. Therefore, the TiO_2 (001) superlattice crystal plane is constructed, and a theoretical simulation study is carried out.

The Cambridge Serial Total Energy Package (CASTEP) module in Materials Studio (MS) is used for DFT calculations [29]. The OTFG ultra-soft pseudopotential is used to describe the electron-ion interaction. The process of electron exchange-correlation can be described using the Generalized Gradient Approximation (GGA) [30] and Perdew–Burke–Ernzerhof (PBE) methods [31]. The electron wave function is extended by the plane wave basis vector group. During all simulations, the cutoff energy is set to 800 eV. Under these conditions, total energy convergence can be achieved. The smaller k-point grid size determined by the k-point convergence test is $3 \times 3 \times 1$, and the convergence values of energy and force are approximately 0.05 eV/Å and 5.0×10^{-6} eV/atom. The supercell model corresponding to the TiO_2 (001) plane is established with 48 atoms, which includes 32 O atoms and 16 Ti atoms. The lateral views of Figure 2 and Figure 3 reveal that the top three layers are not fixed, while the bottom nine layers are fixed. The crystal plane of TiO_2 formed before hydroxylation consists of twelve layers of atoms, and the hydroxyl groups formed after hydroxylation and the adsorbed molecule are set free. Table 1 presents the changes in the bond length attributable to the restructuring of the crystal planes.

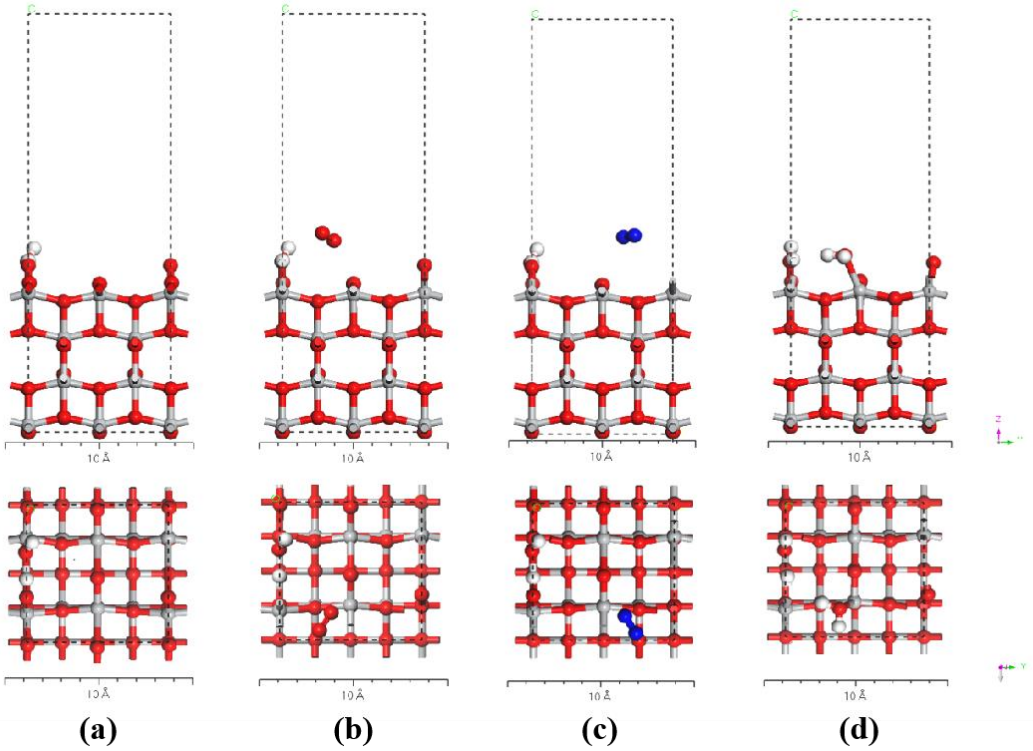

Figure 2 (a-d) Side and top views of the stable structure of the OH-TiO_2 (001) crystal plane before (a) and after the absorption of O_2 (b), N_2 (c), and H_2O (d), respectively. Here, the gray, red, white, and dark blue balls represent Ti, O, H, and N atoms, respectively.

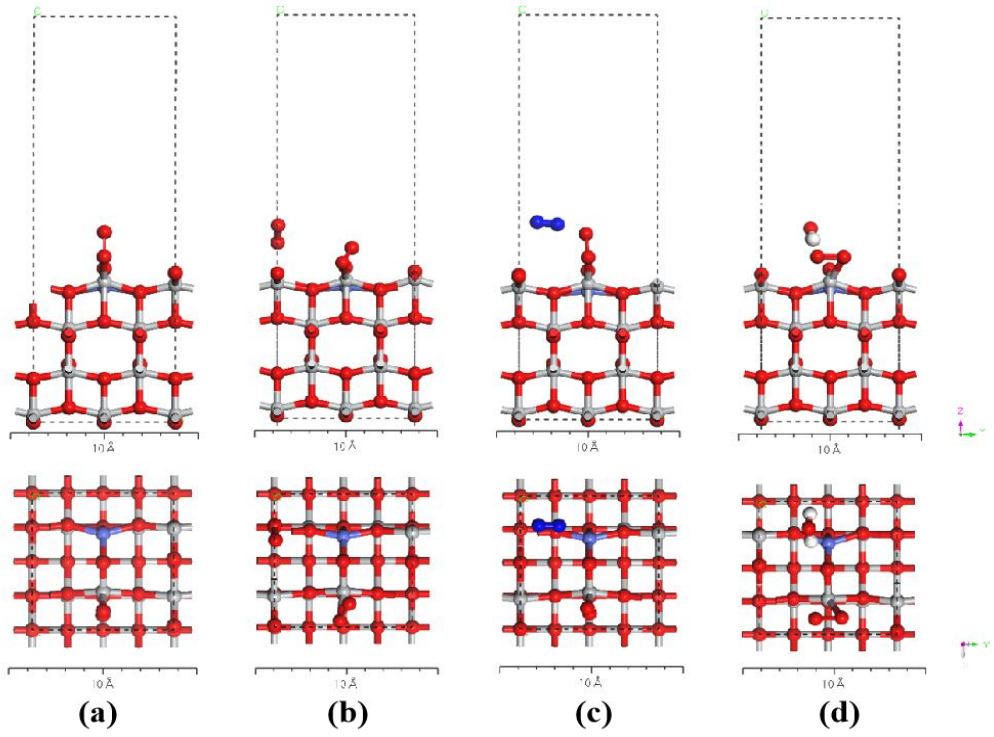

Figure 3 (a-d) Side and top views of the stable structure of the TiO_2-Co (001) crystal plane before (a) and after the absorption of O_2 (b), N_2 (c), and H_2O (d), respectively. Here, the gray, red, white, blue, and dark blue balls represent Ti, O, H, Co, and N atoms, respectively.

Table 1 Changes in the bond length attributable to the changes in the crystal plane structure.

Models		Parallel crystal plane direction bond length/Å			Vertical bond length/Å		
		Bulk	Plane	Changes	Bulk	Plane	Changes
OH-TiO_2 (001)	Ti-OH	/	1.760	/	/	1.760	/
			1.904			1.904	
	Ti-O	1.930	1.751	-0.179	1.973	1.985	0.012
			1.753	-0.177		1.990	0.017
			1.755	-0.175		2.001	0.028
			1.760	-0.170		2.003	0.030
			1.834	-0.096		2.028	0.055
			2.424	0.312		2.034	0.061
						2.068	0.095
						2.085	0.112
TiO_2-Co (001)	Co-O	/	1.773	/	/	1.786	/
			1.880				
	Ti-O_2	/	1.828	/	/	1.828	/
	Ti-O	1.930	1.769	-1.161	1.973	1.907	-0.066
			1.778	-0.152		1.914	-0.059
			1.927	-0.003		1.976	0.003
			1.962	0.032		1.979	0.006
			1.965	0.035		2.088	0.115
			2.142	0.212			

The results of structural optimization reveal that the crystal plane of TiO_2 (001) is characterized by high surface energy. Under these conditions, H_2O molecules are captured and dissociated in the synthesis environment to form hydroxylated planes, labeled OH-TiO_2 (001). Figure 2 (a-d) presents the side and top views of the stable structure of the OH-TiO_2 (001) crystal plane before (a) and after the absorption of O_2 (b), N_2 (c), and H_2O (d), respectively. Here, the gray, red, white, and dark blue balls represent the Ti, O, H, and N atoms, respectively. The OH-TiO_2 (001) crystal plane is derived from the crystal plane TiO_2 (001) after the adsorption of the H_2O molecules and hydroxylation. Following the adsorption of the H_2O molecules on the TiO_2 (001) crystal plane, the OH-TiO_2 (001) crystal plane is obtained following the process of structural optimization. Hence, the atomic composition of the OH-TiO_2 (001) supercell can be expressed as $H_2Ti_{16}O_{33}$.

Following the process of structural optimization, an O vacancy was formed on the crystal plane of Co^{2+} doped TiO_2 (001). Under these conditions, an O_2 molecule is chemically adsorbed near the O vacancy. The heat-treatment environment of the sample makes the process of adsorption of the O_2 molecule stable, and this stable structure is labeled TiO_2-Co (001). Table 2 shows the influence of the adsorbent molecules on the nearest Ti atom distance between the O_2 molecule and the crystal

plane at the inherent oxygen defect of the TiO_2-Co crystal plane. Figure 3 (a-d) shows the side and top views of the stable structure of the TiO_2-Co (001) crystal plane before (a) and after the absorption of O_2 (b), N_2 (c), and H_2O (d) molecules, respectively. Here, the gray, red, white, blue, and dark blue balls represent the Ti, O, H, Co, and N atoms, respectively. A comparison of Figure 3(a) and Figure 3(b)-(d) reveals that the planar atoms of the crystal are reconstructed following the process of structural optimization. Analysis of Figure 3 (a, b) reveals that the atoms on the surface of the crystal plane are characterized by an overall translation which indicates that high energy is required to realize the stable adsorption of the O_2 molecules. In the process of constructing the crystal adsorption model, to prevent the interaction between layers, a vacuum of thickness 15 Å is set along the z-axis, which is used as the molecular adsorption calculation space. Following the optimization of the structure, the positions of the atoms on the surface of the crystal plane change. The arrangement observed under these conditions is different from the arrangement of the atoms in the bulk material. In addition, it can be seen from Table 1 that the Ti-O bond length in the parallel direction of the OH-TiO_2 crystal plane becomes significantly smaller, and the individual becomes significantly large. However, the individual Ti-O bond lengths in the direction parallel to the TiO_2-Co crystal planes decrease significantly. As a whole, the lengths do not increase. This reveals that the bond length changes significantly after the hydroxylation of the crystal plane, and the bond length of the crystal plane changes significantly following the process of Co^{2+} doping.

Table 2 Effect of the adsorbate molecules on the distance between the nearest Ti atoms in the isomorphic plane of the chemisorbed O_2 molecule at the intrinsic oxygen defect of the TiO_2-Co crystal plane.

Models	Adsorbed molecules	nearest facet atom	Bond length/Å	change value/Å
Before molecular adsorption	/	Ti	1.828	/
After molecular adsorption	O_2	Ti	1.950	0.122
	N_2	Ti	1.809	-0.019
	H_2O	Ti	1.918	0.090

The adsorption energy of different gas molecules on the crystal plane of undoped TiO_2 and TiO_2–Co (001) is calculated as follows:

$$E_{ads} = E_{sys} - E_{sur} - E_{gas},$$

where Esys, Esur, and Egas are the total energy after adsorption, the surface energy before adsorption, and the adsorbed gas molecular energy, respectively. Eads indicates the adsorption energy, a negative value indicates the occurrence of an exothermic process, and a positive value indicates the progress of an endothermic process. The larger the negative value, the stronger the interaction.

3. Results and Discussion

3.1 XRD and SEM Analysis

Analysis of the XRD patterns reveals the structure of the prepared anatase titanium dioxide nanocrystals. The diffraction peaks appear at the (2θ) values of 25.32°, 37.04°, 37.82°, 38.58°, 48.07°, 53.82°, 55.08°, 62.80°, 68.83°, 70.23°, 75.14°, and 76.08° (Figure 4). These peaks can be attributed to the (101), (103), (004), (112), (200), (105), (211), (204), (116), (220), (215), and (301) crystal planes, respectively. The results are consistent with those reported by the standard card (PDF#21–1272), indicating that the product is anatase TiO_2. As a result of doping, the diffraction peak corresponding to TiO_2 moves as a result of Co^{2+} doping. This proves that Co^{2+} successfully enters the crystal plane lattice and forms a stable doped crystal plane.

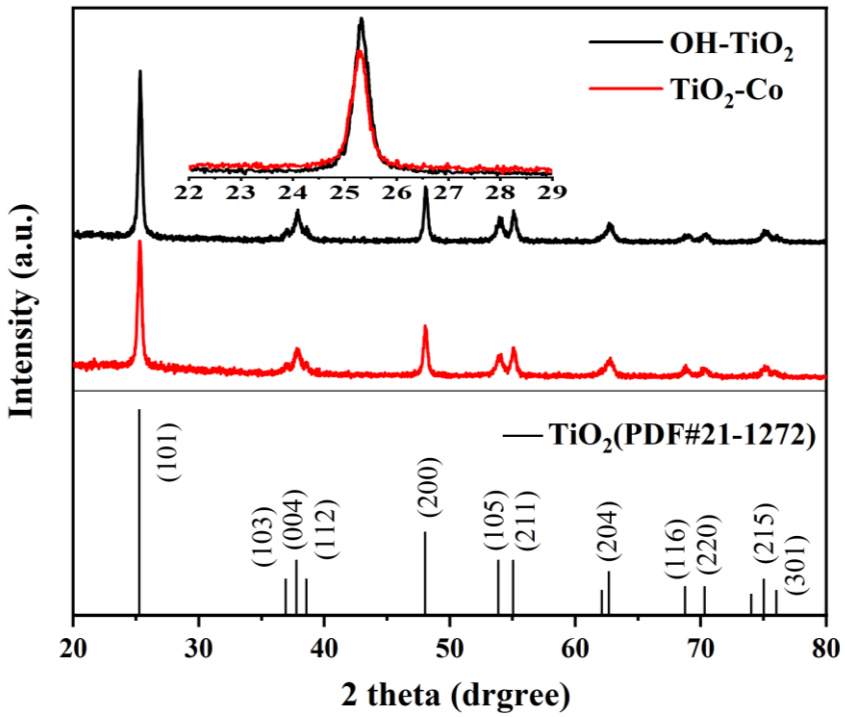

Figure 4 XRD patterns recorded for the undoped TiO_2 and Co^{2+}-doped TiO_2 systems.

Scherrer's formula can be expressed as D = Kλ/Bcosθ. As the diffraction angle θ decreases, the particle size becomes decreases, indicating the shrinkage of the anatase TiO_2 nanosurface lattice.

The SEM and EDS profiles recorded for the anatase TiO_2 system doped with Co^{2+} are shown in Figure 5. The truncated octahedral anatase TiO_2 material, whose particle size is approximately in the range of 30–50 nm, exhibits a flake-like structure (Figure 5. (a)), and the exposed square surface is a high-energy (001) plane. The shape is consistent with the shape reported previously [27]. However, the size reported by us does not agree with the previously reported size. The distribution of the Co, O, and Ti elements is shown in Figure 5 (b), Figure 5 (c), and Figure 5 (d), respectively. EDS results show that Co^{2+} is successfully modified and evenly distributed.

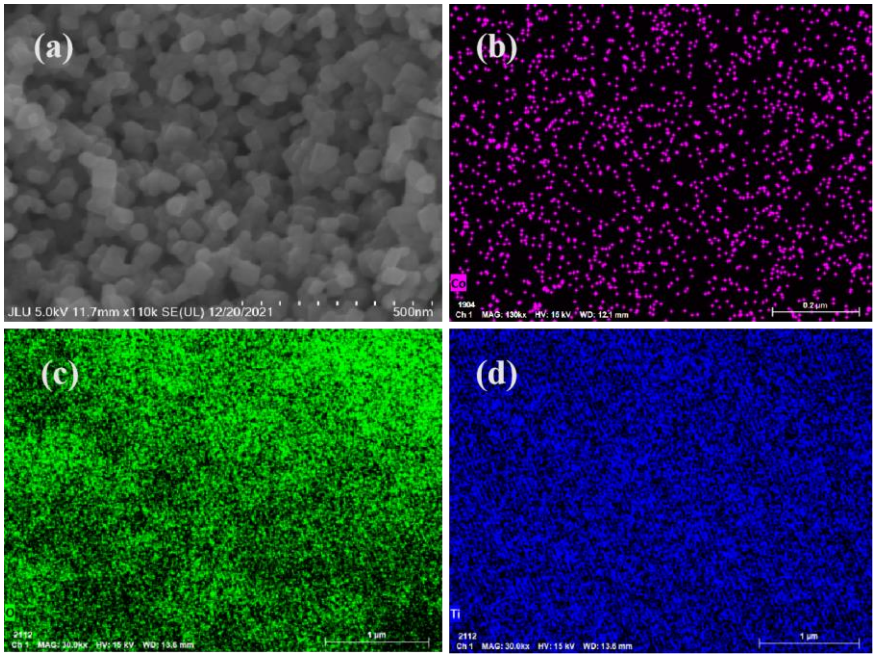

Figure 5 SEM images (a) and EDS (b-d) profiles recorded for TiO_2 doped with Co^{2+}. Subfigures (b), (c), and (d) correspond to the distribution of the Co, O, and Ti elements, respectively.

3.2 FTIR Analysis

FTIR profiles recorded for OH-TiO_2 and TiO_2-Co before and after treatment in air, O_2, and highly humid atmospheres are shown in Figure 6. The infrared spectral profiles recorded for OH-TiO_2 and TiO_2–Co reveal the presence of a wide band between 400 and 750 cm^{-1}. The band is when several bands attributed to various vibration modes of Ti-O and Ti-O-Ti in TiO_2 overlap [32]. Absorption peaks at 669 cm^{-1} and 914 cm^{-1} are related to the adsorption of O_2 molecules. It can be seen that the peak intensity of the peaks recorded in air, highly humid atmosphere, and oxygen atmosphere gradually increases, and the order of peak intensity remains unchanged before and after doping. The presence of the narrow peak at 1631 cm^{-1} can be attributed to the vibration of the physically adsorbed H_2O molecules (H-O-H and Ti-OH bonds) [33]. The profiles recorded for OH-TiO_2 and TiO_2-Co reveal the presence of absorption peaks at 3745 cm^{-1}. These peaks are attributed to the tensile vibration of the surface hydroxyl group (-OH). As can be seen from the figure (Figure 6), the upward peak near 3500 cm^{-1} is related to the adsorption of the H_2O molecule, and the intensity of this peak is inversely proportional to the adsorption amount of the H_2O molecule. The order of adsorption capacity of the H_2O molecules (from low to high) in different atmospheres is oxygen, high humidity air, and air. In addition, the peak intensity before and after doping follows the same order. The adsorption capacity of the H_2O molecule is opposite to that of the O_2 molecule, which indicates that the adsorption of the two gas molecules (O_2 and H_2O molecule) on the crystal plane before and after doping proceeds through the same active site. However, for the crystal plane of TiO_2-Co, this result is contrary to the calculated result. Although the calculated result reveals that the crystal plane of TiO_2–Co contains various active sites, competitive adsorption is observed for the two gas molecules as the distance between the two active sites is short. Therefore, the results are the same as those obtained by studying the TiO_2 crystal planes containing a similar active site. The different ionic

charges of the Ti and Co^{2+} ions result in the replacement of the Ti^{4+} by Co^{2+} units, resulting in the generation of oxygen vacancies that balances charge neutrality. In the TiO_2 lattice, Ti^{4+} is replaced to form a Co-O bond. Thus, the FTIR spectrum can be used as a tool to understand the formation of Co-O bonds in the TiO_2 lattice and the formation of oxygen defects during the substitution of lattice Ti^{4+} by Co^{2+} species [34].

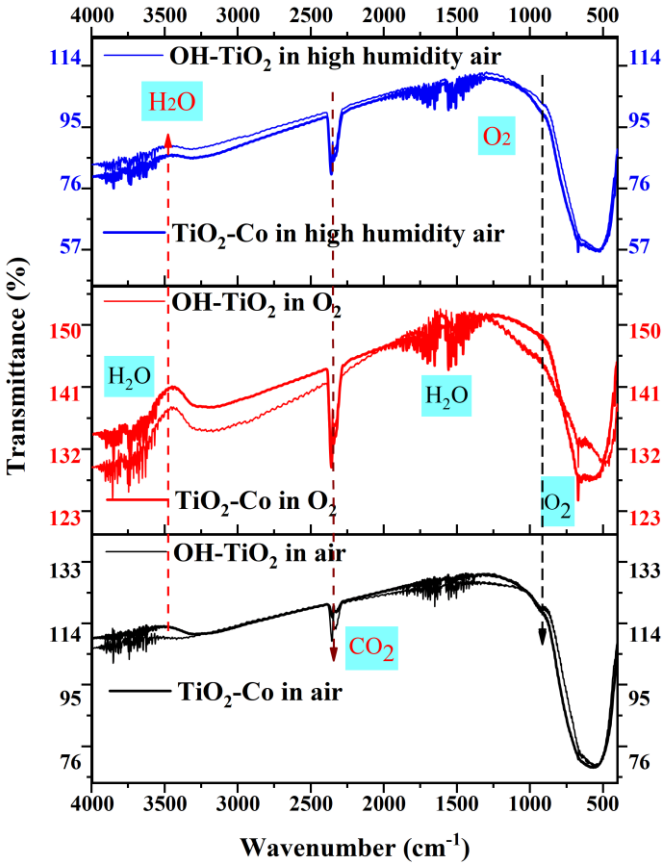

Figure 6 FTIR profiles recorded for undoped TiO_2 and Co^{2+}-doped TiO_2 before and after being placed in air, oxygen, and highly humid environments.

3.3 Result and Discussion

3.3.1 Analysis of CAS and Adsorption Energy

The density of states at the Fermi level correlates positively with the conductivity of the crystal plane. Hence, the change in conductivity is reflected by the density of states at the Fermi level. Table 3 shows the adsorption energies, and Fermi-level density of states of different gas molecules adsorbed on the OH-TiO_2 and TiO_2-Co (001) crystal planes. Table 4 shows the nearest atomic spacing parameters corresponding to the crystal plane when OH-TiO_2 and TiO_2-Co (001) are adsorbed by different gas molecules. It can be seen from the calculation results (Table 3) that H_2O molecules are strongly chemisorbed and adsorbed by hydrogen bonds. Therefore, the H_2O molecule is identified as the characteristic adsorption species. The theoretically synthesized OH-TiO_2 (001) crystal plane not only contains hydroxyl groups but also exhibits the ability to chemisorb H_2O molecules. This indicates that the crystal plane is only sensitive to the adsorption and desorption reactions of H_2O molecules. Due to the adsorption of O_2 molecules, the Fermi-level density of states of the crystal

plane increases from 3.57 electrons/eV to 5.04 electrons/eV, indicating that the spontaneous adsorption of O_2 molecules would result in an increase in the conductivity of the crystal plane. The conductivity of the other two molecules is not significantly reduced under these conditions.

Table 3 Adsorption energies and Fermi-level density of states for the adsorption of different gas molecules on the OH-TiO_2 and TiO_2-Co (001) crystal planes.

OH-TiO_2 (001)	DOS of Fermi (electrons/eV)	Adsorption energy (electrons/eV)	Adsorption type
/	3.57	/	/
N_2	3.59	-0.049	physics
O_2	5.04	-0.064	physics
H_2O	3.50	-1.278	chemistry hydrogen bond
TiO_2-Co (001)			
/	5.85	/	/
N_2	12.00	1.430	physics
O_2	11.40	-1.392	chemistry
H_2O	13.00	-5.334	Chemical hydrogen bond

Table 4 Nearest atomic distance between the crystal planes of OH-TiO_2 and TiO_2-Co (001) and adsorbed molecules.

Models	Adsorbed molecules	nearest facet atom	Distance/Å
OH-TiO_2 (001)	O_2	Ti	3.145
	N_2	Ti	3.477
	H_2O	Ti	2.190
TiO_2-Co (001)	O_2	Ti	2.028
	N_2	O	3.185
	H_2O	O	2.304

During the chemical synthesis process, O_2 molecules in the air are captured by defect sites. Hence, O_2 molecules are identified as the characteristic adsorption species of the Co^{2+}-doped TiO_2 (001) crystal plane. It can be seen from Table 3 that the adsorption of all three molecules results in an increase in the crystal conductivity of TiO_2-Co (001). The adsorption energy of N_2 is 1.430 electron/eV (see Table 3), which indicates that the N_2 molecules cannot be re-adsorbed following desorption. The adsorption energy of the O_2 and H_2O molecules on the crystal plane are –1.392 electron/eV and –5.334 electron/eV, respectively (Table 3). The results reflect chemical adsorption.

3.3.2 Electron Density Difference (EDD)

Figure 7 (a, b) and Figure 7 (c, d) present the side view (top) and top view (bottom) of the molecular adsorption system (EDD; Isovalue = 0.1) before and after Co^{2+} doping on the TiO_2 (001) plane. The adsorption molecules presented in (a, c) and (b, d) are O_2 and H_2O molecules, respectively.

Yellow and blue indicate electron outflow and inflow, respectively. It can be seen from Figure 7 that the O_2 molecule is physically adsorbed on the hydroxylated TiO_2 (001) crystal plane, the O_2 molecule is chemisorbed when TiO_2 (001) crystal plane is doped with Co^{2+}, and the H_2O molecule is chemisorbed before and after doping. This is consistent with the results obtained for the OH-TiO_2 (001) crystal plane-based chemisorption of H_2O molecule (Table 3) and the results obtained for the Co^{2+}-doped crystal plane-based chemisorption for O_2 and H_2O molecules (Table 3).

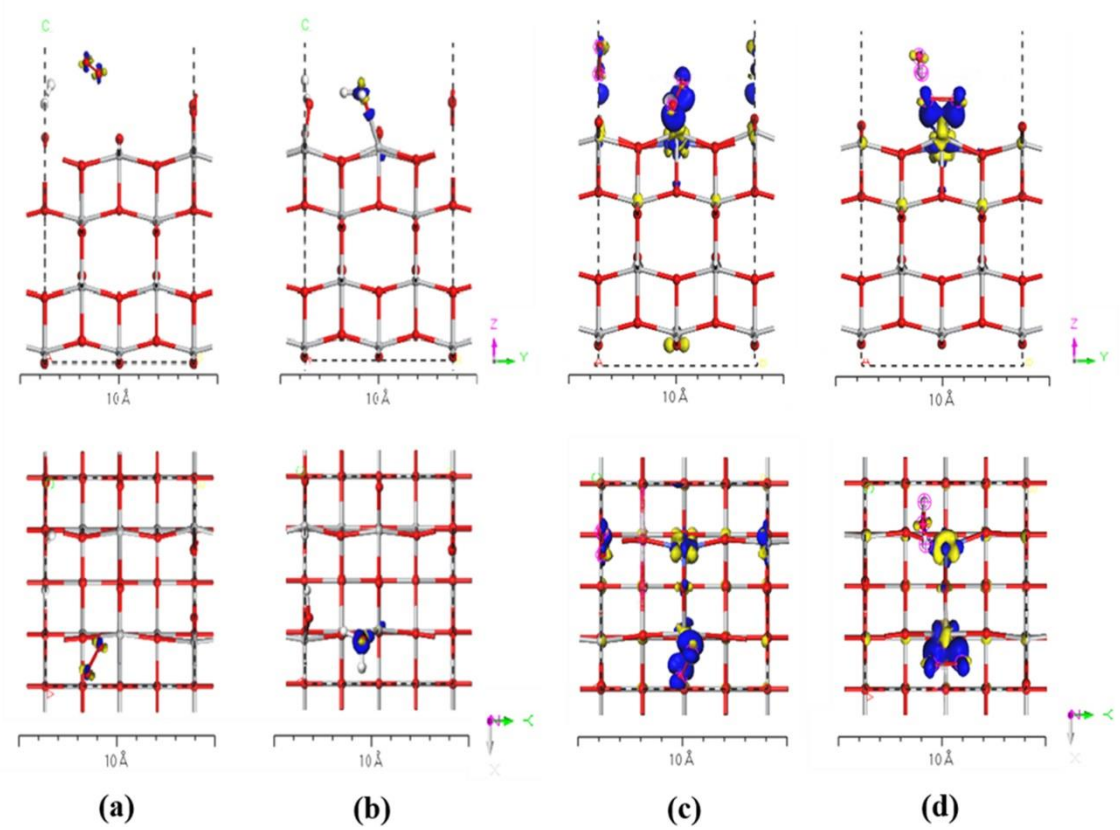

Figure 7 Lateral (top) and top view (bottom) of EDD (Isovalue = 0.1) of molecular adsorption system before (a, b) and after (c, d) doping the TiO_2 (001) crystal plane with Co^{2+}. The adsorption molecules of (a, c) and (b, d) are O_2 and H_2O molecules, respectively. Yellow and blue indicate electron outflow and inflow, respectively.

3.3.3 EIS Analysis

Figure 8 presents the EIS profiles presenting the adsorption stability of OH-TiO_2 and TiO_2-Co in air. The introduction of Co^{2+} ions significantly increases the conductivity of the crystal plane. The simulation results reveal that the Fermi level density of states of the Co^{2+}-doped TiO_2 crystal plane increases from 3.57 electrons/eV to 5.85 electrons/eV. Figure 8 (a) and Figure 8 (b) are equivalent fitting circuit diagrams corresponding to OH-TiO_2 and TiO_2-Co, respectively. Figure 8 (b) reveals that the equivalent circuit is divided into Rp and Warburg impedance. Rp plays a major role under conditions of high frequency, and the current is controlled by dynamic processes. Warburg impedance plays a major role in low-frequency regions and is related to the diffusion mechanism. It has been reported that the Warburg impedance of crystals is potentially related to the contribution of oxygen vacancies on the crystal plane at low frequencies [35, 36]. According to the

structure optimization model of TiO_2-Co, Co^{2+} ion doping results in the formation of oxygen vacancies on the crystal plane. This is consistent with experimental results.

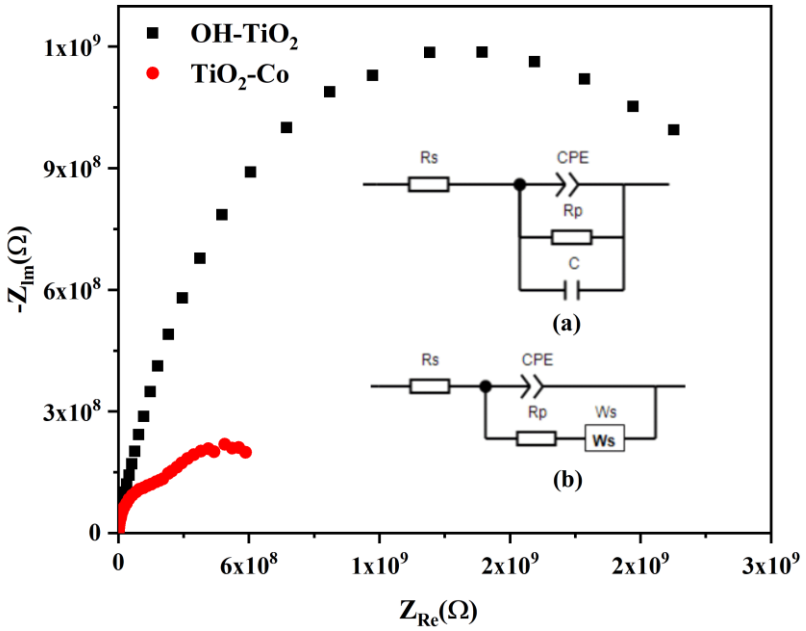

Figure 8 EIS profiles recorded for OH-TiO_2 and TiO_2-Co in air. Equivalent fitting circuits corresponding to OH-TiO_2 (a) and TiO_2-Co (b).

Figure 9 presents the EIS profiles recorded for OH-TiO_2 following the process of vacuum treatment in N_2, O_2, and H_2O atmospheres conducted for 120, 100, and 120 min, respectively. The experimental results show that the adsorption of the three gases results in an increase in the conductivity of the crystal plane. Experimental and theoretical simulation results reveal that the adsorption of N_2, O_2, and H_2O causes the Fermi level state density of the OH-TiO_2 (001) crystal plane to change from 3.57 electron/eV to 3.59 electron/eV, 5.04 electron/eV, and 3.50 electron/eV. The change in the crystal plane conductivity is not obvious as the adsorption of N_2 and H_2O molecules is observed. Under these conditions, the adsorption of O_2 increases the crystal plane conductivity significantly, which is consistent with the experimental results.

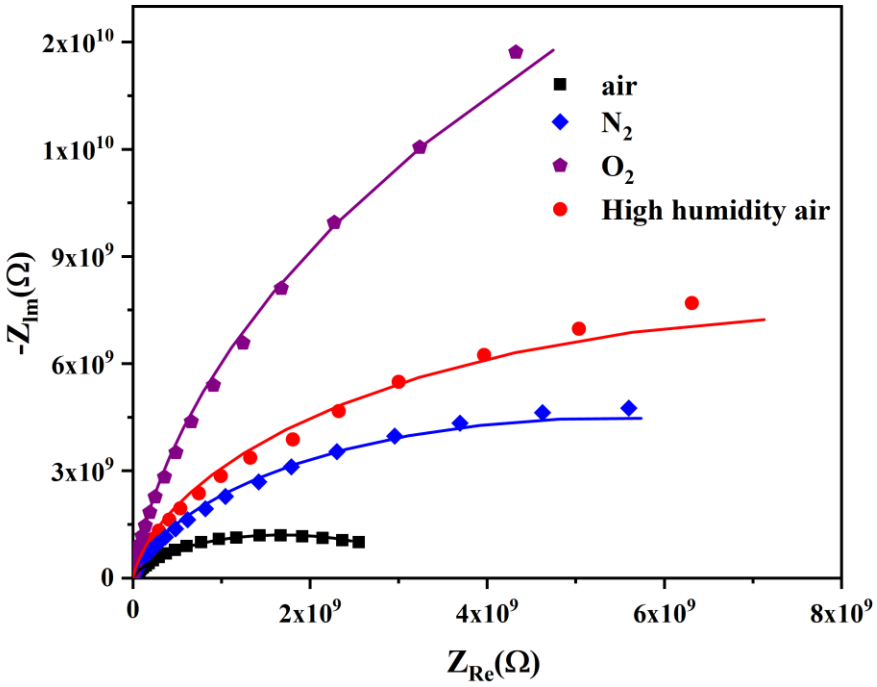

Figure 9 EIS profiles recorded for OH-TiO_2 (001) in air, N_2, O_2, and highly humid conditions (all points present the experimental data, and the lines present the fitting data).

Figure 10 presents the changes in the Rp curve. The data were fitted from the EIS curve of OH-TiO_2 (001)-based adsorption in air, N_2, O_2, and highly humid air. According to the theoretical simulation results, single-molecule H_2O is adsorbed on the crystal plane, and the process exerts little effect on the conductivity of the TiO_2 (001) crystal plane. However, the continuously adsorbed H_2O molecules are hydrogen-bonded to form H_2O molecular aggregates, which are naturally adsorbed on the synthetic TiO_2 (001) crystal plane resulting in the generation of electrical conductivity [37]. As the adsorption of N_2 molecules has little contribution to the conductivity (Table 3), in the N_2 environment, the random movement and collision of N_2 molecules reduce the extent of formation of H_2O molecular aggregates in the crystal plane. Under these conditions, the conductivity of the crystal plane decreases. The amount of H_2O molecular aggregates is significantly reduced when they are exposed to the vacuum state for 12 h. This results in a further decrease in the crystal plane conductivity. The conductivity is significantly improved in the O_2 molecular environment, which is consistent with the fact that the Fermi level density of states increases from 3.57 electrons/eV to 5.04 electrons/eV (Table 3).

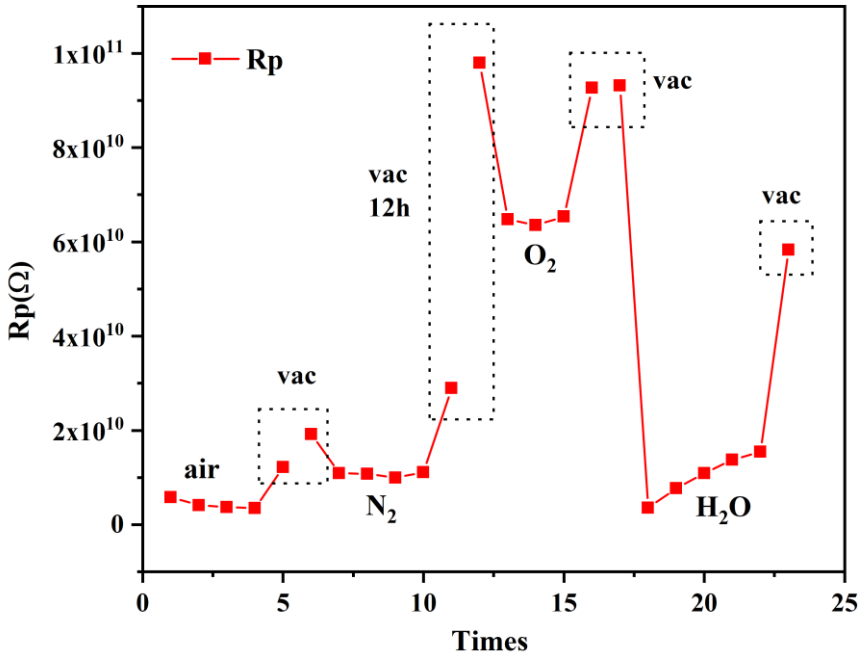

Figure 10 Changes in the Rp curve are fitted by the EIS curve of the OH-TiO_2 (001) adsorption process in air, N_2, O_2, and high humidity air.

The simultaneous existence of N_2 and O_2 molecules in high humidity air results in a rapid increase in the conductivity of the crystal, and the Fermi level density of states increases from 3.57 electrons/eV to 5.04 electrons/eV. Due to the random movement of N_2 and O_2 molecules, they collide with the condensing H_2O molecular aggregates, resulting in the gradual adsorption of the condensing H_2O molecules. The process continues until stability is attained. The density of states of the Fermi level decreases from 5.04 electrons/eV to 3.50 electrons/eV. Therefore, from the calculation results and EIS results, it can be seen that the H_2O molecular aggregates have a significant effect on the increase in the crystal plane conductivity. The contribution is much larger than the contribution of the process of adsorption of O_2 molecules. A significant effect is observed on the crystal plane conductivity.

Figure 11 (i) and Figure 11 (ii) present the EIS profiles of the TiO_2-Co crystal recorded in air and high humidity air, respectively. All points represent the experimental data, and the lines represent the fitting data. Under conditions of the air test environment (Figure 11 (i)), the crystal conductivity increases with the adsorption of gas. The Fermi level densities of the N_2, O_2, and H_2O states increase from 5.85 electrons/eV to 12.00 electrons/eV, 11.40 electrons/eV, and 13.00 electrons/eV, respectively. The doping of Co^{2+} ions results in the formation of natural O defects on the TiO_2-Co crystal plane. Hence, there are three crystal plane modes of the TiO_2-Co crystal in the vacuum state, namely, the TiO_2-Co crystal plane O vacancy mode, the H_2O-TiO_2-Co mode, and the O_2-TiO_2-Co mode. As shown in Figure 11 (ii), the 120 min-long treatment process conducted in a vacuum results in a significant reduction in the H_2O molecular aggregates on the crystal plane. Under these conditions, the electrical conductivity decreases significantly. Hence, even in a highly humid environment, the electrical conductivity on the TiO_2-Co crystal plane cannot recover to the value recorded in the air.

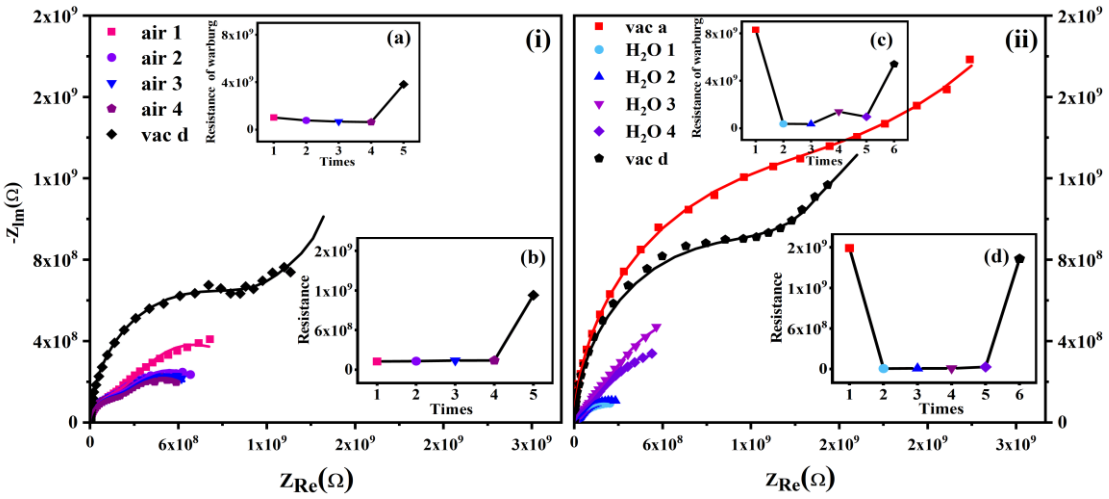

Figure 11 EIS profiles recorded for TiO_2-Co (001) before and after adsorption in air and highly humid conditions. (a)(c) present the Ws values of the fitting curve, (b)(d) present the Rp values of the fitting curve. (All points represent experimental data, and the lines represent fitting data).

Figure 12 (i) and Figure 12 (ii) present the EIS profiles corresponding to the adsorption–desorption process of N_2 and O_2 molecules on the TiO_2-Co (001) crystal plane. For the process of N_2 gas adsorption, it can be seen from Figure 12 (i) that N_2 adsorption increases the conductivity of the crystal plane, and the simulation results show that N_2 adsorption increases the Fermi level state density from 5.85 electrons/eV to 12.00 electrons/eV. However, the process of endothermic adsorption of N_2 molecules hinders the progress of the process at room temperature(25°C). The direct adsorption of N_2 molecules does not contribute significantly to the electrical conductivity of the crystal plane. The movement of N_2 molecules results in the desorption of the H_2O molecular aggregates on the crystal plane, resulting in changes in the conductivity of the crystal plane. It can be seen that the conductivity of the crystal plane decreases significantly before and after N_2 treatment. In addition, the EIS fitting data (Figure 12 (ii)) reveals that the adsorption of O_2 molecules cannot be predicted by the calculation results (Table 3). This indicates that the O_2 molecules cannot be stably adsorbed on the crystal planes. A comparison of Figure 3 (a) and Figure 3 (b) reveals that the stable adsorption of O_2 requires a large amount of energy to reform the crystal planes. This is difficult to achieve spontaneously at room temperature(25°C). Therefore, the adsorption–desorption behavior of O_2 molecules is consistent with that of the N_2 molecules.

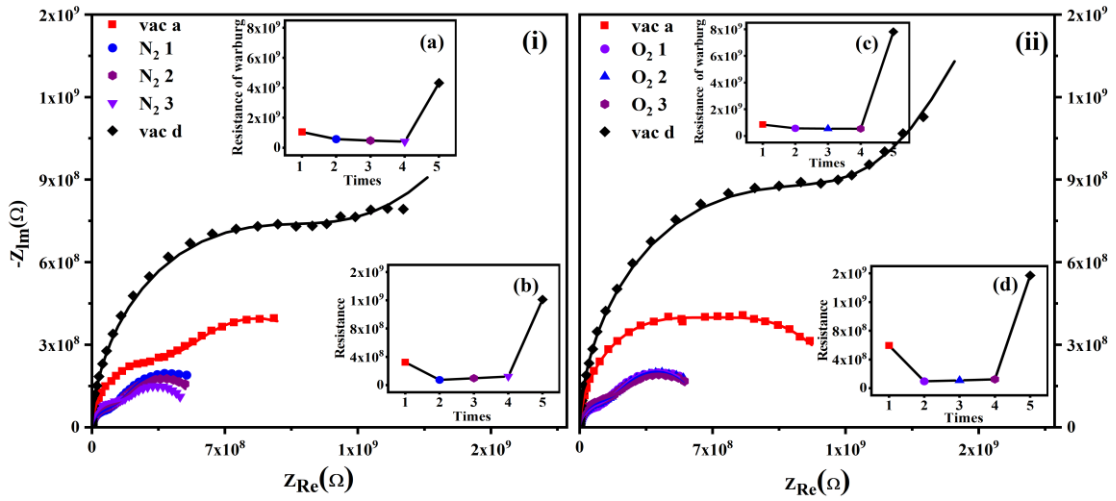

Figure 12 EIS profiles recorded for TiO_2-Co (001) before and after the adsorption in N_2 and O_2 environments. (a)(c) present the Ws value of the fitting curve, and (b)(d) present the Rp value of the fitting curve. (All points represent experimental data, and the lines represent the fitting data).

4. Conclusions

The adsorption behavior of O_2, N_2, and H_2O molecules on TiO_2 (001) and TiO_2-Co (001) crystal planes in air is simulated using the DFT technique. The results show that H_2O molecules are captured and dissociated on TiO_2 (001) to form hydroxylated crystal structures, which further adsorb H_2O molecules through hydrogen bonds to form characteristic adsorbed species. The doping of Co^{2+} ions results in the formation of oxygen vacancies on the TiO_2 (001) crystal planes. The O_2 molecules are chemically adsorbed on the TiO_2-Co (001) crystal plane. When adequate amounts of O_2 is present, O_2 molecules continue to get chemically adsorbed on the crystal plane. Among the three molecules, the O_2 molecule increased the conductivity of OH-TiO_2, while all the three gas molecules increased the conductivity of the crystal plane doped with Co^{2+}. The presence of H_2O molecular aggregates increases the conductivity of two crystal planes. The optimization results of the structural model of molecular adsorption reveal that the three molecules exhibit competitive adsorption properties on the OH-TiO_2 (001) crystal plane. Adsorption competition is not observed between the O_2 and H_2O molecules on the TiO_2-Co (001) crystal plane. However, the process of adsorption is potentially affected as the adsorption sites for the two molecules are situated in close proximity. These results are confirmed using the FTIR and EIS techniques. This indicates that Co^{2+} doping can change the electrical properties of the TiO_2 (001) crystal plane and improve the adsorption capacity of O_2. The results reveal the influence of the process of natural molecular adsorption on the surface conductivity and adsorption properties of synthetic crystals. The results reported herein can potentially help in the development of catalysts and gas-sensitive materials.

Acknowledgments

This paper is dedicated to the 70th anniversary of the physics of Jilin University.

Author Contributions

JiaRui Fang: Conceptualization, Methodology, Software, Investigation, Data curation, Supervision, Writing-Original draft preparation. Ziheng Li*: Supervision, Software. Xiruo Bai, Yichu Zhang: Visualization, Validation, Writing-Reviewing, and Resources. Jiahui Liu, Dan Wang, Ye Yao: Validation, Writing-Reviewing, and Editing.

Competing Interests

The authors declare that they have no known competing financial interests or personal relationships that could have appeared to influence the work reported in this paper.

References

1. Meng RS, Cai M, Jiang JK, Liang QH, Sun X, Yang Q, et al. First principles investigation of small molecules adsorption on antimonene. IEEE Electron Device Lett. 2017; 38: 134-137.
2. Mao Z, Lei T, He Y, Cai Z, Xiong Y, Zhang S. Accumulated chemical adsorption phenomenon of H_2 on mox gas sensor under temperature programmed cooling. IEEE Sens J. 2017; 17: 2784-2791.
3. Li Q, Zhu X, Song H, Chen W, Zhang Q, Peng H. Gas adsorption characteristics of graphene/metal contact structures. Appl Surf Sci. 2020; 514: 145823.
4. Zhu W, Qian W, Liu R, Huang W, Luo H, Dong C. Field emission energy distribution studies of single multi-walled carbon nanotube emitter with gas adsorptions. Vacuum. 2022; 199: 110933.
5. Zhao P, Li T, Zhang D. Adsorption of dissolved gas molecules in the transformer oil on silver-modified (002) planes of molybdenum diselenide monolayer: A DFT study. J Phys Condens Matter. 2021; 33: 485201.
6. Gui Y, Li W, He X, Ding Z, Tang C, Xu L. Adsorption properties of pristine and Co-doped TiO_2(1 0 1) toward dissolved gas analysis in transformer oil. Appl Surf Sci. 2020; 507: 145163.
7. Lin L, Shi Z, Yan L, Tao H, Yao L, Li S, et al. First-principles study of CO adsorption on Os atom doped anatase TiO_2 (1 0 1) surface. Polyhedron. 2020; 191: 114814.
8. Shi Z, Lin L, Chen R, Yan L. Adsorption of CO molecules on anatase TiO_2 (001) loaded with noble metals M (M = Ir/Pd/Pt): A study from DFT calculations. Mater Today Commun. 2021; 28: 102699.
9. Wang M, Jin C, Luo Q, Kim EJ. Sol-gel derived TiO_2–carbon composites with adsorption-enhanced photocatalytic activity and gas sensing performance. Ceram Int. 2020; 46: 18608-18613.
10. Zeng W, Liu T, Wang Z. Impact of Nb doping on gas-sensing performance of TiO_2 thick-film sensors. Sens Actuators B. 2012; 166-167: 141-149.
11. Panta R, Nanthamathee C, Ruangpornvisuti V. Adsorption of hydrogen and hydrogen–containing gases on Pd–and Ag–single atoms doped on anatase TiO_2 (1 0 1) surfaces and their sensing performance. Appl Surf Sci. 2018; 450: 112-121.
12. Chen Y, Yu L, Du H, Hu C, Liu N, Ma S, et al. Hierarchical flower-like TiO_2 microspheres for high-selective NH_3 detection: A density functional theory study. Sens Actuators B. 2021; 345: 130303.
13. Abbasi A, Sardroodi JJ. Molecular design of O_3 and NO_2 sensor devices based on a novel heterostructured N-doped TiO_2/ZnO nanocomposite: A van der Waals corrected DFT study. J Nanostruct Chem. 2017; 7: 345-358.

14. Sivachandiran L, Thevenet F, Gravejat P, Rousseau A. Investigation of NO and NO_2 adsorption mechanisms on TiO_2 at room temperature. Appl Catal B. 2013; 142-143: 196-204.
15. Dong X, Zhang X, Cui H, Zhang J. A first principle simulation of competitive adsorption of SF6 decomposition components on nitrogen-doped anatase TiO_2 (101) surface. Appl Surf Sci. 2017; 422: 331-338.
16. Wang W, Liu F, Wang B, Wang Y. Effect of defects in TiO_2 nanoplates with exposed {001} facets on the gas sensing properties. Chin Chem Lett. 2019; 30: 1261-1265.
17. Yang Y, Hong A, Liang Y, Xu K, Yu T, Shi J, et al. High-energy {001} crystal facets and surface fluorination engineered gas sensing properties of anatase titania nanocrystals. Appl Surf Sci. 2017; 423: 602-610.
18. Sui Y, Wu L, Zhong S, Liu Q. Carbon quantum dots/TiO_2 nanosheets with dominant (001) facets for enhanced photocatalytic hydrogen evolution. Appl Surf Sci. 2019; 480: 810-816.
19. Wanbayor R, Ruangpornvisuti V. Adsorption of CO, H_2, N_2O, NH_3 and CH_4 on the anatase TiO_2 (0 0 1) and (1 0 1) surfaces and their competitive adsorption predicted by periodic DFT calculations. Mater Chem Phys. 2010; 124: 720-725.
20. Lin L, Shi Z, Huang J, Wang P, Yu W, He C, et al. Molecular adsorption properties of CH_4 with noble metals doped onto oxygen vacancy defect of anatase TiO_2 (1 0 1) surface: First-principles calculations. Appl Surf Sci. 2020; 514: 145900.
21. Abbasi A, Sardroodi JJ. A novel nitrogen dioxide gas sensor based on TiO_2-supported au nanoparticles: A van der Waals corrected DFT study. J Nanostruct Chem. 2017; 7: 121-132.
22. Aguilera-Granja F, Aguilera-del-Toro RH, Vogel EE, Cisternas E. TiO_2 nano-clusters adsorbed on surfaces: A density-functional-theoretic study. J Phys Chem Solids. 2021; 150: 109716.
23. Potapenko DV, Li Z, Osgood RM. Photoreactions on a single isolated TiO_2 nanocrystal on Au(111): Photodecomposition of TMAA. J Phys Chem C. 2015; 119: 28946-28953.
24. Malik AS, Liu T, Rittiruam M, Saelee T, Da Silva JLF, Praserthdam S, et al. On a high photocatalytic activity of high-noble alloys Au–Ag/TiO_2 catalysts during oxygen evolution reaction of water oxidation. Sci Rep. 2022; 12: 2604.
25. Goliaei EM, Seriani N. Structure and electronic properties of small silver–gold clusters on titania photocatalysts for H_2O_2 production: An investigation with density functional theory. J Phys Chem C. 2019; 123: 2855-2863.
26. Aguilera-Granja F, Aguilera-del-Toro RH, Vogel EE, Cisternas E. Bimetalic (AuPt) 4 nano-clusters adsorbed on TiO_2 nano-wires: A density-functional-theoretic study. J Phys Chem Solids. 2021; 159: 110275.
27. Shao C, Lin L, Duan L, Jiang Y, Shao Q, Cao H. Nickel-enhanced electrochemical activities of shape-tailored TiO_2{001} nanocrystals for water treatment: A combined experimental and DFT studies. Electrochim Acta. 2021; 376: 138066.
28. Li H, Liu H, Zhang Q, Wang C, Tianduo L. Synthesis and photocatalytic activity of ring-like anatase TiO_2 with {001} facts exposed. Ceram Int. 2015; 41: 8717-8722.
29. Lv H, Gao H, Yang Y, Liu L. Density functional theory (DFT) investigation on the structure and electronic properties of the cubic perovskite $PbTiO_3$. Appli Catal A. 2011; 404: 54-58.
30. Gong J, Yang C, Zhang J, Pu W. Origin of photocatalytic activity of W/N-codoped TiO_2: H_2 production and DFT calculation with GGA+U. Appl Catal B. 2014; 152-153: 73-81.
31. Morales-García Á, Valero R, Illas F. Reliable and computationally affordable prediction of the energy gap of $(TiO_2)_n$ ($10 \leq n \leq 563$) nanoparticles from density functional theory. Phys Chem

Chem Phys. 2018; 20: 18907-18911.
32. El Mragui A, Zegaoui O, Daou I, Esteves da Silva JCG. Preparation, characterization, and photocatalytic activity under UV and visible light of Co, Mn, and Ni mono-doped and (P,Mo) and (P,W) co-doped TiO_2 nanoparticles: A comparative study. Environ Sci Pollut Res. 2021; 28: 25130-25145.
33. Senthilkumar V, Kathalingam A, Kannan V, Senthil K, Rhee JK. Reproducible resistive switching in hydrothermal processed TiO_2 nanorod film for non-volatile memory applications. Sens Actuators A. 2013; 194: 135-139.
34. Zhu L, Zeng Y, Zhang S, Deng J, Zhong Q. Effects of synthesis methods on catalytic activities of CoOx–TiO_2 for low-temperature NH_3-SCR of NO. J Environ Sci. 2017; 54: 277-287.
35. Grunbaum N, Dessemond L, Fouletier J, Prado F, Mogni L, Caneiro A. Rate limiting steps of the porous $La_{0.6}Sr_{0.4}Co_{0.8}Fe_{0.2}O_{3-\delta}$ electrode material. Solid State Ionics. 2009; 180: 1448-1452.
36. Mogni L, Grunbaum N, Prado F, Caneiro A. Oxygen reduction reaction on Ruddlesden–Popper phases studied by impedance spectroscopy. J Electrochem Soc. 2010; 158: B202.
37. Li ZL, Yi XH, Liu R, Bi JJ, Fu HY, Zhang GP, et al. Effect of H_2O adsorption on negative differential conductance behavior of single junction. Sci Rep. 2017; 7: 4195.